J. Fluid Mech. (1983), *vol.* 137, *pp.* 165–186
Printed in Great Britain

Measurement of streamwise vorticity fluctuations in a turbulent channel flow

By ELEFTERIOS G. KASTRINAKIS† AND HELMUT ECKELMANN
Max-Planck-Institut für Strömungsforschung, Göttingen, West Germany

(Received 5 February 1982 and in revised form 10 February 1983)

In a fully developed turbulent channel flow, measurements of the streamwise vorticity fluctuations ω_x have been made. A newly designed probe provides simultaneously in addition to the vorticity signal all three velocity signals. The new probe bears a likeness to the Kovasznay-type vorticity probe, but consists of four electrically independent hot wires, each mounted separately on a total of eight supporting prongs. A new calibration technique had to be developed for this probe.

In addition to various statistical properties of the three velocity components, the distributions of vorticity fluctuations and of skewness and flatness factors are given up to wall distances as close as $y^+ = 19$. A pronounced maximum of the streamwise vorticity fluctuations was found at $y^+ \approx 20$. Large values of the flatness factor characterize the outer flow region.

1. Introduction

Turbulent shear flow has been studied in the past 15 years with respect to coherent structures. Visual studies carried out by Hama (Corrsin 1957), Kline *et al.* (1967), Corino & Brodkey (1969) and Kim, Kline & Reynolds (1971) provided the first impulse in this direction. There is today no longer any doubt that coherent structures are a major component in turbulent flows. They play an important part in the production, dissipation and transport of turbulent energy.

An important structural element in wall-bounded turbulent flows is the vortex-like structure that has been observed by various investigators using different experimental techniques. Theodorsen (1952) was the first to postulate a horseshoe-like vortical structure; Willmarth & Tu (1967) were also able to explain their wall-pressure velocity correlations with the existence of a horseshoe vortex. Finally Bakewell & Lumley (1967) proposed a counterrotating vortex pair near the wall. The visual studies by Praturi & Brodkey (1978), Brodkey (1978), Falco (1980) and Head & Bandyopandhyay (1981), and also the hot-film investigation by Blackwelder & Eckelmann (1979) all indicate the existence of streamwise vortex-like structures in the vicinity of the wall. Recently Smith *et al.* (1980) were able to observe the development of streamwise vortices and simultaneously estimate their intensities with the help of the hydrogen-bubble method. However, it has as yet neither been possible to substantiate the existence of these streamwise vortices nor to measure their vorticity by means of hot-wire anemometers. A first step in this direction was

† Permanent address: Department of Chemical Engineering, Institute of Technology, University of Thessaloniki, Greece.

made by Frish & Webb (1981), who employed a new optical method to measure the vorticity in a laminar channel flow.

The idea for a probe allowing direct measurement of the streamwise component of vorticity stems from Kovasznay (1950, 1954). Uberoi & Corrsin (1951) used such a probe to investigate the propagation of turbulence into an adjacent laminar flow. Kistler (1952) employed this probe in isotropic turbulence, and Corrsin & Kistler (1955) used the probe to investigate the boundary between a turbulent boundary layer and the adjacent potential flow field. Willmarth and Tu (see Willmarth 1975), Kastrinakis (1977) and Kastrinakis *et al.* (1978) investigated wall-bounded turbulent shear flow with a Kovasznay probe. In these measurements the vorticity signal is influenced by the three velocity components, as Kastrinakis, Eckelmann & Willmarth (1979) were later able to show. Since the Kovasznay probe also measures the streamwise velocity component U, the influence of this component can be corrected instantaneously with the help of a computer. A correction for the two transverse components v and w of velocity is not possible, as these cannot be measured with this probe. A new probe allowing the simultaneous measurement of all three *velocity* components along with the streamwise *vorticity* component was suggested by Kastrinakis *et al.* (1979). Such a probe was constructed by Cleveland (1979) and later used by Vukoslavcevic & Wallace (1981) to investigate the influence of the velocity gradients $\partial u/\partial y$ and $\partial u/\partial z$ on the vorticity signal.

In this paper a new vorticity probe constructed at the Max-Planck-Institut für Strömungsforschung is first described. The probe allows the simultaneous measurement of all three velocity components and the streamwise vorticity component. Secondly, a calibration technique developed for this probe is introduced which takes the influence of all three velocity components on the vorticity signal into account. Finally, measurements carried out in a fully developed turbulent channel flow are described.

2. Operation of the vorticity probe

A probe for the direct measurement of the streamwise component $\omega_x = \partial w/\partial y - \partial v/\partial z$ of the vorticity vector is sketched in figure 1. The probe resembles the vorticity probe originally suggested by Kovasznay in that it consists of four hot wires, which in our case are all inclined at an angle of 35° with respect to the probe axis. The four hot wires are operated independently from each other, in contrast with the operation of a Kovasznay-type probe, where the wires are all interconnected and constitute a Wheatstone bridge. Since the new vorticity probe requires eight instead of four prongs as in the Kovasznay probe, its construction becomes more complicated. Each hot wire of the new probe is supported independently by two prongs. Thus the array resembles two X-probes which are oriented perpendicularly to each other. Figure 2 shows a photograph of a probe tip. For comparison a 10 mm scale is also given. The eight

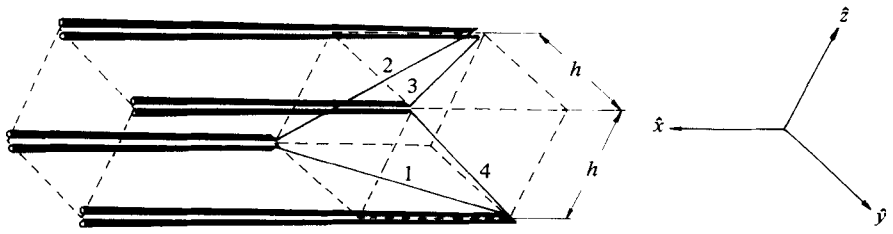

FIGURE 1. Schematic of the vorticity probe.

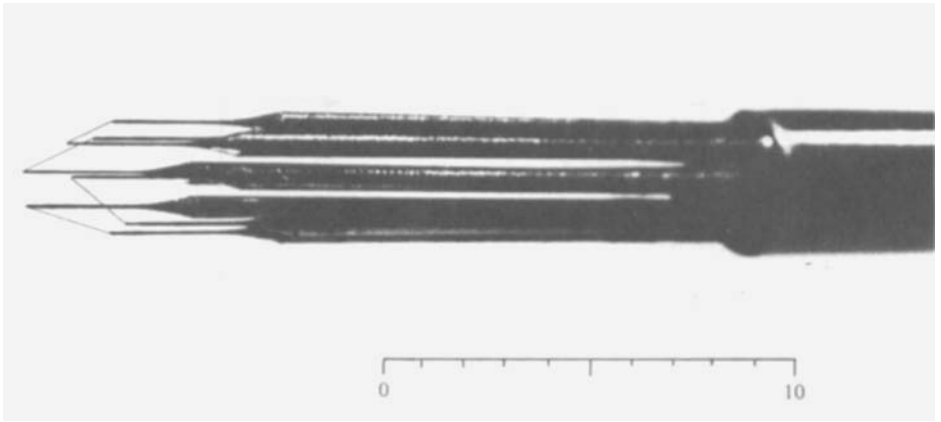

FIGURE 2. Photograph of the vorticity-probe tip.

prongs of the probe are made of 0.6 mm steel rods which are ground at the tips over a length of 3 mm to a diameter of 0.1 mm. An increase in the size of the new probe in comparison with the Kovasznay probe originally used by Kastrinakis *et al.* (1979) was not necessary. The probe diameter is 4 mm in both cases. The hot wires of the new probe are 5 μm in diameter and about 1.5 mm long. They consist of platinum-plated tungsten wire, and are welded on the prongs. The distance h between the wires shown in figure 1 is 1.9 mm. More details of the probe construction are given in figure 3.

In the following calculations, two different Cartesian coordinate systems are used, which are fixed either with respect to the flow field (x, y, z) or the probe $(\hat{x}, \hat{y}, \hat{z})$. Hot wires 1 and 3 lie in the $(\hat{x}, \hat{y})$-plane at different $\hat{z}$-coordinates; hot wires 2 and 4 lie in the $(\hat{x}, \hat{z})$-plane at different $\hat{y}$-coordinates. Their projections in the $(\hat{x}, \hat{y})$- and $(\hat{x}, \hat{z})$-planes are shown in figure 4. The four hot wires are inclined at angles α to δ with respect to the $\hat{x}$-axis (probe axis). Orientation of the probe is generally such that its coordinate system coincides with that of the flow field, in which the mean velocity $\overline{U}$ and the three fluctuating velocity components u, v, w are defined. Since each of the four hot wires has a length-to-diameter ratio of 300, it can be assumed that only the velocity component normal to a wire contributes to its cooling. The effective cooling speeds can then be calculated as:

$$U_{K1} = \{[(\overline{U}_1 + u_1)\sin\alpha + v_1\cos\alpha]^2 + w_1^2\}^{\frac{1}{2}},$$
$$U_{K2} = \{[(\overline{U}_2 + u_2)\sin\beta + w_2\cos\beta]^2 + v_2^2\}^{\frac{1}{2}},$$
$$U_{K3} = \{[(\overline{U}_3 + u_3)\sin\gamma - v_3\cos\gamma]^2 + w_3^2\}^{\frac{1}{2}},$$
$$U_{K4} = \{[(\overline{U}_4 + u_4)\sin\delta - w_4\cos\delta]^2 + v_4^2\}^{\frac{1}{2}}.$$

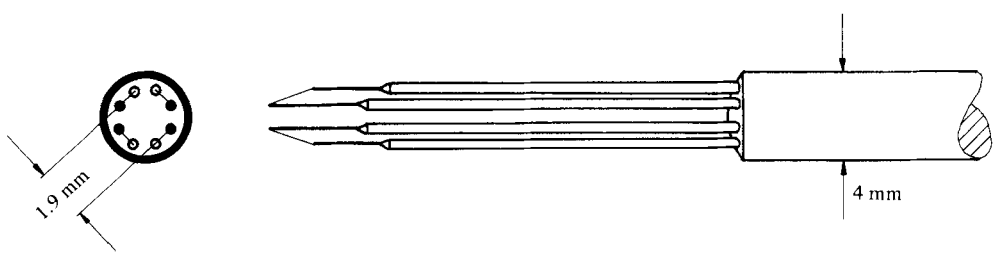

FIGURE 3. Sketch of the vorticity probe.

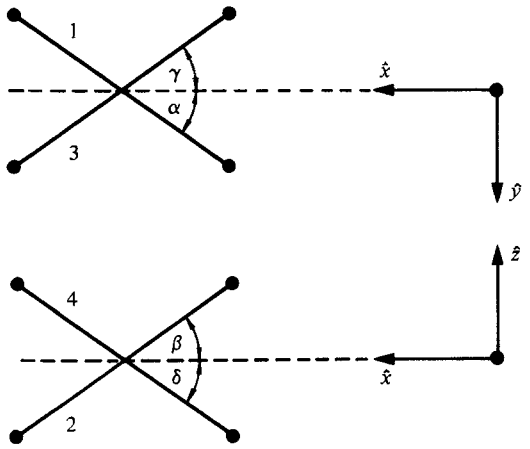

FIGURE 4. Arrangement of the hot wires.

The indices $1, \ldots, 4$ indicate the velocity components at the position of the respective hot wire. Thus for example U_1 and U_3 or w_1 and w_3 need not be equal, as the hot wires 1 and 3 lie in two different planes. With the assumption that $U_1 \gg u_i, v_i, w_i$ $(i = 1, \ldots, 4)$, the terms in braces can be expanded in Taylor series. If the expansion is truncated after the second-order term, it then follows that

$$U_{K1} \approx \sin\alpha\left(\overline{U}_1 + u_1 + v_1\cot\alpha + \frac{w_1^2}{2\overline{U}_1\sin^2\alpha}\right), \tag{1a}$$

$$U_{K2} \approx \sin\beta\left(\overline{U}_2 + u_2 + w_2\cot\beta + \frac{v_2^2}{2\overline{U}_2\sin^2\beta}\right), \tag{1b}$$

$$U_{K3} \approx \sin\gamma\left(\overline{U}_3 + u_3 - v_3\cot\gamma + \frac{w_3^2}{2\overline{U}_3\sin^2\gamma}\right), \tag{1c}$$

$$U_{K4} \approx \sin\delta\left(\overline{U}_4 + u_4 - w_4\cot\delta + \frac{v_4^2}{2\overline{U}_4\sin^2\delta}\right). \tag{1d}$$

Before the three velocity components $\overline{U}+u$, v and w and the vorticity component ω_x can be calculated as linear combinations of the cooling speeds $U_{K1}, \ldots, U_{K4}$ which are measured directly, these speeds must be referred to the probe axis. This is accomplished through a series expansion around a point on the probe axis corresponding to the centre of gravity of the four wires, which is indicated in the following by a suffix 0. When (1*a–d*) are expanded up to first-order terms, one obtains

$$U_{K1} = \sin\alpha\left[(\overline{U}_0 + u_0) - \frac{\partial(\overline{U}+u)}{\partial z}\bigg|_0\frac{h}{2} + \left(v_0 - \frac{\partial v}{\partial z}\bigg|_0\frac{h}{2}\right)\cot\alpha + \frac{w_1^2}{2\overline{U}_1\sin^2\alpha}\right], \tag{2a}$$

$$U_{K3} = \sin\beta\left[(\overline{U}_0 + u_0) - \frac{\partial(\overline{U}+u)}{\partial y}\bigg|_0\frac{h}{2} + \left(w_0 - \frac{\partial w}{\partial y}\bigg|_0\frac{h}{2}\right)\cot\beta + \frac{v_2^2}{2\overline{U}_2\sin^2\beta}\right], \tag{2b}$$

$$U_{K3} = \sin\gamma\left[(\overline{U}_0 + u_0) + \frac{\partial(\overline{U}+u)}{\partial z}\bigg|_0\frac{h}{2} - \left(v_0 + \frac{\partial v}{\partial z}\bigg|_0\frac{h}{2}\right)\cot\gamma + \frac{w_3^2}{2\overline{U}_3\sin^2\gamma}\right], \tag{2c}$$

$$U_{K4} = \sin\delta\left[(\overline{U}_0 + u_0) + \frac{\partial(\overline{U}+u)}{\partial y}\bigg|_0\frac{h}{2} - \left(w_0 + \frac{\partial w}{\partial y}\bigg|_0\frac{h}{2}\right)\cot\delta + \frac{v_4^2}{2\overline{U}_4\sin^2\delta}\right]. \tag{2d}$$

The above equations provide the basis for calculating the streamwise component of vorticity, where the sum of (2*b*) and (2*d*) is subtracted from the sum of (2*a*) and (2*c*):

$$\omega_x = \frac{\partial w}{\partial y} - \frac{\partial v}{\partial z} = \frac{2}{Bh}\left[\frac{U_{K1}}{\sin\alpha} + \frac{U_{K3}}{\sin\gamma} - \frac{U_{K2}}{\sin\beta} - \frac{U_{K4}}{\sin\delta} - v(\cot\alpha - \cot\gamma) + w(\cot\beta - \cot\delta) - \frac{w^2 - v^2}{\bar{U}\sin^2\tilde{\alpha}}\right]. \quad (3)$$

The suffix 0 has now been omitted. Further simplification of the expression was made possible by use of the following symbols:

$$B \equiv \cot\alpha + \cot\gamma \approx \cot\beta + \cot\delta,$$
$$\bar{U}\sin^2\tilde{\alpha} \equiv \bar{U}_1\sin^2\alpha \approx \bar{U}_2\sin^2\beta \approx \bar{U}_3\sin^2\gamma \approx \bar{U}_4\sin^2\delta$$

for $\alpha \approx \beta \approx \gamma \approx \delta \approx \tilde{\alpha}$, which is valid for our probe. Equation (3) shows the influence of both normal components v and w on the vorticity signal ω_x. The quadratic term in v and w does not vanish, even when all four probe angles are equal. Vukoslavcevic & Wallace (1981) have also pointed this out. Thus the influence of v and w on the vorticity signal must be taken into account during probe calibration.

Exact measurements of the three velocity components require that the distance h between hot wires (figure 1) and the Kolmogoroff length η satisfy the inequality

$$\frac{h}{\eta} \leqslant 1, \quad (4)$$

i.e. the distance between hot wires must be chosen smaller than the smallest structural element occurring in the flow. In order to measure the vorticity component ω_x with the same probe, this distance must be chosen greater than the Kolmogoroff length. In this case h should satisfy the inequality

$$1 < \frac{h}{\eta} \lesssim 3.33, \quad (5)$$

according to measurements by Wyngaard (1969), i.e. h must be larger than the smallest-occurring eddy in order that a gradient be measurable, while at the same time h must not exceed 3.3 times the eddy size. Equations (4) and (5) cannot be satisfied simultaneously. Our experimental results show, however, that velocity measurements are possible with the new vorticity probe even though (4) cannot be satisfied. For the turbulent channel flow investigated, the Kolmogoroff length η can be estimated from the dissipation per unit mass

$$\epsilon = 2\tau_w L(H+2b)\frac{0.9U_{CL}}{\rho LH2b},$$

with $U_{CL} = 200$ cm/s, $u_\tau = (\tau_w/\rho)^{\frac{1}{2}} \approx 9$ cm/s, channel height $H = 140$ cm, channel width $2b = 18$ cm and channel length L. We find

$$\eta = \left(\frac{\nu^3}{\epsilon}\right)^{\frac{1}{4}} \approx 0.4 \text{ mm},$$

with $\nu = 0.15$ cm^2/s for air. The resulting relationship $h/\eta = 4.8$ is thus only slightly larger than the value suggested by Wyngaard, (5); however, when h is expressed in wall units, a value $h^+ = hu_\tau/\nu \approx 11.5$ results. This limits the use of the probe to wall distances that are greater than about twice this value.

3. Testing of the new vorticity probe

3.1. *The vorticity probe as a velocity meter*

The new vorticity probe was first used for velocity measurements in a known fully developed turbulent channel flow. The probe was operated in constant-temperature mode by four TSI anemometers with an overheat ratio $R_w/R_k = 1.3$ for each of the hot wires, corresponding to a temperature difference of approximately 75 °C. This temperature difference was chosen in order to ensure that the convection produced by the hot-wire sensors would remain as small as possible and so that the frequency response of the hot wires would still be sufficiently high.

The wind tunnel (figure 5) used for the measurements was the former rough-walled tunnel of the MPI für Strömungsforschung, which possesses a closed test section (*a*) of length $L = 9.5$ m and an open-flow return. The channel width $2b$, originally measuring 28 cm, had to be reduced to 18 cm to increase its relative length from 34 to 53 channel widths. The channel height $H = 140$ cm remained unchanged. Although the relative channel length was about the same as for Comte-Bellot's (1965) investigation, an additional honeycomb along with two trip edges (*b*) had to be positioned at the entrance to the test section. The trip edges consist of two mesh-screen stripes each 3 cm high. They are mounted on each vertical wall of the test section downstream of the honeycomb. In this way a fully developed turbulent flow 51–53 channel widths downstream of the nozzle was achieved, with a centreline velocity of 200 cm/s. The channel fan (*d*) can be driven either by a three-phase a.c. motor with a variable gear system or by a d.c. motor (*e*). The maximum centreline velocity in the test section obtained by the a.c. drive is 10 m/s. With the d.c. motor a maximum speed of 40 m/s can be achieved. To make hot-wire measurements possible in this channel, filter mats (*f*) are used at the channel entrance to trap dust and solid particles carried by the oncoming air.

With the new probe at a location 52 channel widths downstream of the nozzle, both the distribution of the streamwise velocity fluctuations u and the mean-velocity profile could be measured in accordance with the literature. However, the distributions of the two transverse fluctuating velocity components v and w were measured as approximately 20% smaller than expected. In order to better understand these deviations, the new velocity probe was further investigated in a uniform irrotational flow with a turbulence level $(\overline{u^2})^{\frac{1}{2}}/\overline{U} = 0.1\,\%$ existing in the wind tunnel at location

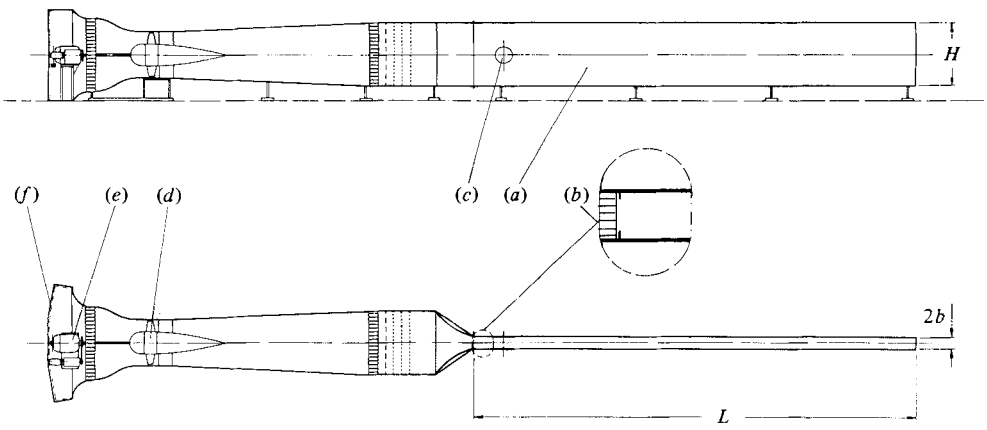

FIGURE 5. Wind tunnel.

(*c*) in figure 5, when both honeycomb and tripping device are removed. Here the two transverse components $\hat{v}$ and $\hat{w}$ in the probe-fixed coordinate system can easily be obtained by yawing ϕ and pitching θ the probe. The three velocity components in the probe-fixed system are

$$\hat{U} = U\cos\phi\cos\theta, \tag{6a}$$

$$\hat{v} = U\sin\phi, \tag{6b}$$

$$\hat{w} = U\cos\phi\sin\theta, \tag{6c}$$

where the vector sum of the three induced components must yield the oncoming flow velocity

$$U = (\hat{U}^2+\hat{v}^2+\hat{w}^2)^{\frac{1}{2}}.$$

For the case where the vorticity probe is first pitched by an angle θ and then yawed by an angle ϕ, it follows that

$$\hat{U} = U\cos\theta\cos\phi, \tag{7a}$$

$$\hat{v} = U\cos\theta\sin\phi, \tag{7b}$$

$$\hat{w} = U\sin\theta. \tag{7c}$$

The velocity components measured with the vorticity probe in a potential flow field follow from (2) with $\alpha = \beta = \gamma = \delta$:

$$\hat{U} = \frac{1}{4\sin\alpha}[(U_{K1}+U_{K3})+(U_{K2}+U_{K4})], \tag{8a}$$

$$\hat{v} = \frac{1}{2\cos\alpha}(U_{K1}-U_{K3}), \tag{8b}$$

$$\hat{w} = \frac{1}{2\cos\alpha}(U_{K2}-U_{K4}). \tag{8c}$$

As U occurs twice, we here use the average of the two values. In addition to the gradients which vanish in a potential flow field, here the quadratic term in $\hat{v}$ and $\hat{w}$, which could occur only in the U-term, has been neglected. However, this term is included in calibration. Equations (8*a–c*) must also be used for the calculation of the three velocity components when measured in the turbulent channel flow, but in this case gradients which occur additionally cannot be measured explicitly with the vorticity probe. We shall return to this problem at the end of this section.

The transverse components $\hat{v}$ and $\hat{w}$ induced by yawing and pitching the vorticity probe in a potential flow field were again too small, as measured previously in the fully developed turbulent channel flow. The vorticity probe was thereupon not only calibrated at the zero angle but in the range of angles $-15° \leqslant \phi, \theta \leqslant +15°$ in order that both transverse components could be taken into account more accurately. All the additional information gained through calibration for different probe orientations other than $\phi = \theta = 0$ was stored in a computer in polynomial form. In order to obtain the actual velocity components at the position of the vorticity probe, the velocity components resulting from (8) must be multiplied by factors c_{U1}, c_{U2}, c_v and c_w respectively, which are calculated from the stored information; in case of U the first parenthesis is multiplied by c_{U1} and the second by c_{U2}.

To illustrate, the dependence of these factors on $\hat{v}$ and $\hat{w}$ is shown in figures 6–9 for $U = 200$ cm/s; in the interest of clarity, only four different transverse velocity

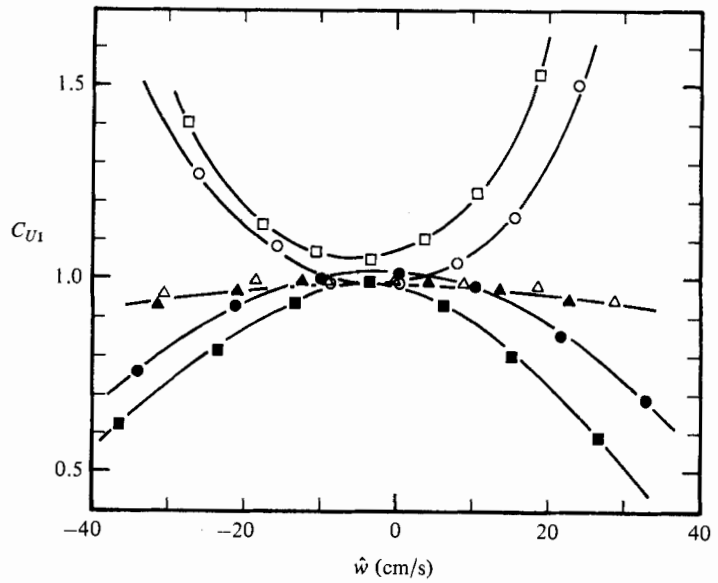

FIGURE 6. Dependence of calibration factor C_{U1} on the two transverse velocity components $\hat{v}$ and $\hat{w}$ for three different mean-flow velocities $\overline{U}$: ○, $\overline{U}$ = 170 cm/s; $\hat{v}$ = 0 cm/s; □, 170 cm/s, 24.9 cm/s; △, 200 cm/s, 0 cm/s; ▲, 200 cm/s, 28.5 cm/s; ●, 230 cm/s, 0 cm/s; ■, 230 cm/s, 32.5 cm/s.

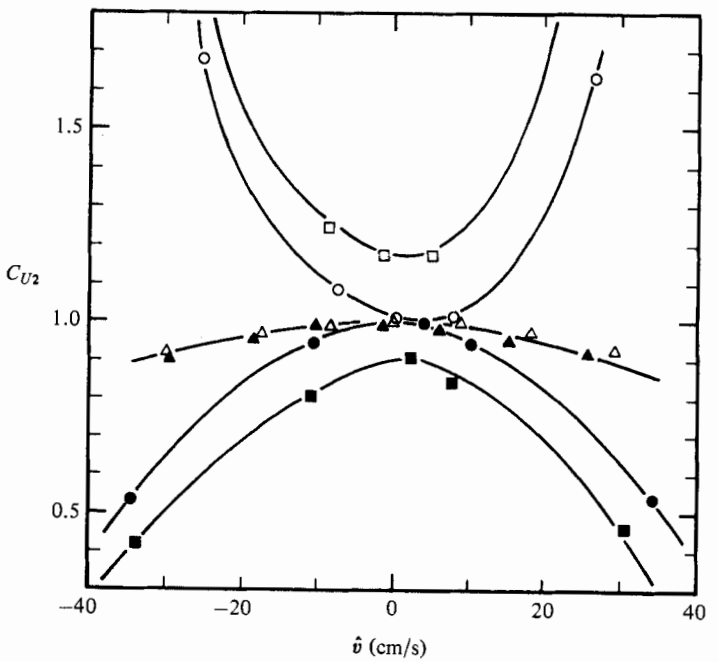

FIGURE 7. Dependence of calibration factor C_{U2} on the two transverse velocity components $\hat{v}$ and $\hat{w}$ for three different mean-flow velocities $\overline{U}$: ○, $\overline{U}$ = 170 cm/s, $\hat{w}$ = 0 cm/s; □, 170 cm/s, 22.3 cm/s; △, 200 cm/s, 0 cm/s; ▲, 200 cm/s, 26.6 cm/s; ●, 230 cm/s, 0 cm/s; ■, 230 cm/s, 30.9 cm/s.

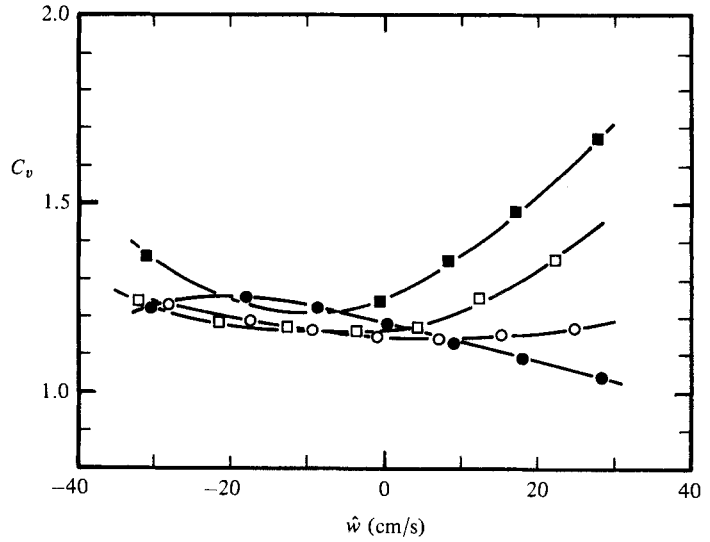

FIGURE 8. Dependence of calibration factor C_v on $\hat{w}$ for $U = 200$ cm/s: ■, $\hat{v} = 7.8$ cm/s; □, 28.5 cm/s; ●, −9.1 cm/s; ○, −29.5 cm/s.

components are considered in each figure. The influence of the streamwise velocity fluctuations $\hat{u} = \hat{U} - U$ on $\hat{v}$ and $\hat{w}$ was also studied. This influence can be neglected when $\hat{u}/\hat{U}$ remains less than $\pm 20\,\%$. Thus the curves illustrated in figure 8 and 9 can be assumed to be independent of U when measurement accuracy is taken into account. The factors c_v and c_w are always greater than unity, except at one point. This is equivalent to previous results in which the measured values of both transverse components were always too small. The streamwise fluctuations measured in the same flow were not in error, since the factors c_{U1} and c_{U2} (figures 6 and 7) are both less than unity for positive and greater than unity for negative fluctuations. Thus the error was cancelled out during the course of an entire measurement, whereas considerable errors appeared in the measurement of instantaneous values. The shapes of the calibration curves for the streamwise velocity component shown in figures 6 and 7 result mainly from the influence of the quadratic terms, which were neglected in (8). The calibration technique applied here also takes the thermal wake of the wires and the wake of the prongs into account when the flow angle is non-zero. The same applies for the factors c_v and c_w. Jerome, Quitton & Patel (1971) have already pointed out the influence of a thermal wake for an X-probe in an oblique flow.

As in the case with all standard X-probes, velocity measurements are adversely influenced by the velocity gradients $\partial U/\partial y$, $\partial U/\partial z$, $\partial v/\partial z$ and $\partial w/\partial y$ present in turbulent flows. Little is known concerning the magnitude of the instantaneous values for these gradients. The maximum values for $\partial U/\partial y$ and $\partial U/\partial z$ have been determined by Eckelmann *et al.* (1977) and recently also by Vucoslavcevic & Wallace (1981). At the smallest wall distance $y^+ = 19$ of the present work, values corresponding roughly to the mean wall gradient $(\partial \overline{U}/\partial y)\,|_{\mathrm{W}}$ were found. If one assumes that the instantaneous values for the other two gradients $\partial v/\partial z$ and $\partial w/\partial y$ can for short periods of time also approach this magnitude, then for short periods an error in the measurement of U, v and w of 25, 100 and 65% respectively would result. It must, however, be emphasized that such an error will always be present when X-probes are used in multicomponent measurements. This error is approximately twice as large for the

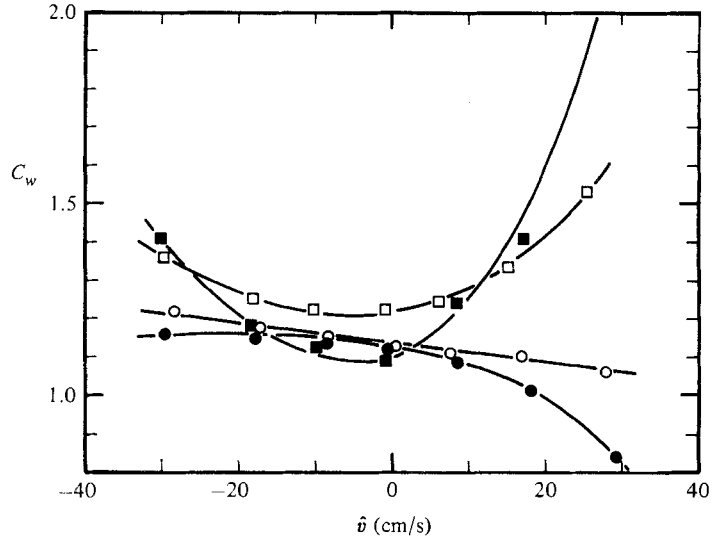

FIGURE 9. Dependence of calibration factor C_w on $\hat{v}$ for $\bar{U} = 200$ cm/s: ■, $\hat{w} = 7.9$ cm/s; □, 26.6 cm/s; ●, −9.8 cm/s; ○, −30.5 cm/s.

vorticity probe as compared with standard X-probes owing to the greater distance between hot wires of the probe. However, the error rapidly becomes smaller with increasing wall distance, as shown in the measurements of Eckelmann *et al.* and Vucoslavcevic & Wallace.

3.2. *The vorticity probe as a vorticity meter*

The influence of the three velocity components on the vorticity signal was also investigated in a potential flow field. Both transverse velocity components v and w can again be induced by yawing and pitching the probe. In order to simulate a fluctuation in the streamwise component, the mean flow velocity was either increased or decreased by $\Delta U = \pm \hat{u}$. According to (3), the probe must measure a non-zero value for ω_x even in a potential flow field where $\omega_x = 0$. The quadratic term in v and w from (3) does not vanish even when the angles α, γ and β, δ are pairwise equal. The dependence of the vorticity signal on the two transverse components is shown in figures 10–12 for a flow speed of $U = 200$ cm/s with $\hat{u} = -30$ cm/s, 0 and +30 cm/s. The quadratic dependence on $\hat{v}$ and $\hat{w}$ can easily be seen in these figures, as expected from (3). As can be easily verified by extrapolating the corresponding curves in figures 10–12 $\omega_{x\mathrm{sp}}$ vanishes for $\hat{v}^2 \approx \hat{w}^2$. The curves also show that the vorticity signal is only slightly dependent on the streamwise velocity component.

While measuring vorticity in a turbulent flow, that part of the vorticity signal due to the three fluctuating velocity components must be known at all times and simultaneously subtracted from the probe signal. This is only possible with the help of a digital computer. We followed the procedure outlined in §3.1 for velocity measurements. The $\omega_{x\mathrm{sp}}$ values obtained during calibration with different speeds U, $\hat{v}$ and $\hat{w}$ in a potential flow field were again stored in the computer as second-order polynomials, and intermediate values not measured during calibration were obtained by a nonlinear interpolation.

The gradients $\partial U/\partial y$ and $\partial U/\partial z$ do not explicitly occur in (3), which defines the streamwise component of vorticity. In spite of the calibration technique employed

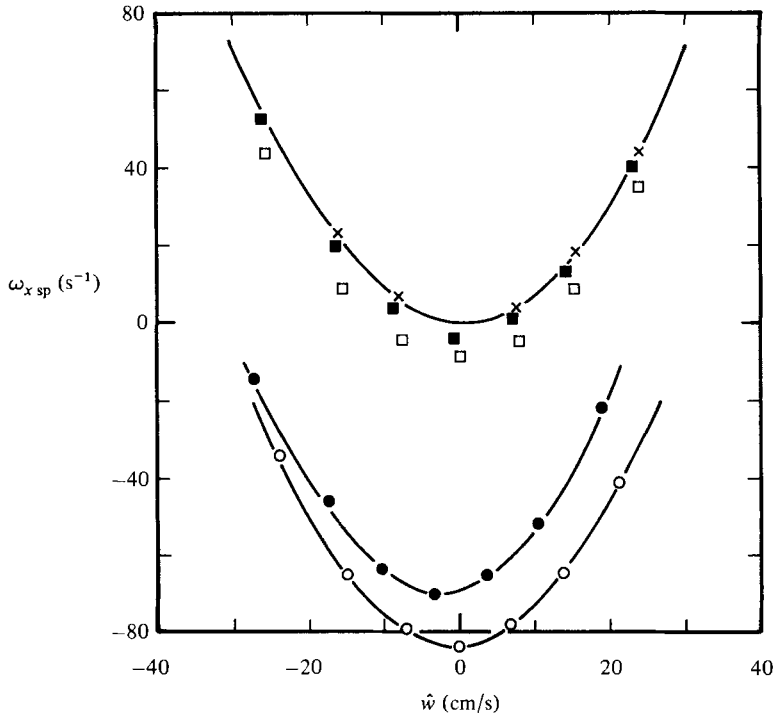

FIGURE 10. Spurious vorticity signal due to the influence of the two transverse velocity components $\hat{v}$ and $\hat{w}$ for $\overline{U} = 170$ cm/s: ■, $\hat{v} = 6.7$ cm/s; ●, 24.9 cm/s; ×, 0 cm/s; □, −7.9 cm/s; ○, −25.6 cm/s.

here, an error in determining ω_x can result, since the instantaneous values of all three velocity components influenced by the gradients $\partial U/\partial y$, $\partial U/\partial z$, $\partial v/\partial z$ and $\partial w/\partial y$ are insufficiently known.

In §3.1 it was shown that at $y^+ = 19$ instantaneous errors as high as 25, 100 and 65% can occur in U, v and w respectively. Such values would cause errors in the instantaneous ω_x of 5, 10 and 15% respectively. This would be a worst-case estimate, which would be reached briefly during a time series, if ever. Since the gradients become smaller at larger wall distances, this error decreases rapidly with increasing wall distance.

4. Measurements of velocity and vorticity in a turbulent channel flow

Measurements based on the calibration scheme described in §3 were again carried out in the turbulent channel flow of the wind tunnel at $U_{CL} = 200$ cm/s. This centreline velocity along with a channel width of $2b = 18$ cm results in a Reynolds number of 25200 for the flow. It was necessary to calibrate the vorticity probe in the range of angles $-15° \leqslant \phi, \theta \leqslant +15°$, taking into account the measurements by Kreplin & Eckelmann (1979) in a similar flow in which the flow angles for distances from the wall of $y^+ = yu_\tau/\nu \gtrsim 15$ were determined. The subsequent measurements were carried out in two stages. First, the instantaneous values $U_{K1}, \ldots, U_{K4}$ for the four hot wires of the vorticity probe were digitized with a frequency of 1 kHz using the sample-and-hold method and then stored on the magnetic disc of a PDP 15 computer. Before digitizing, analog ω_x signals were observed on a storage oscilloscope. The

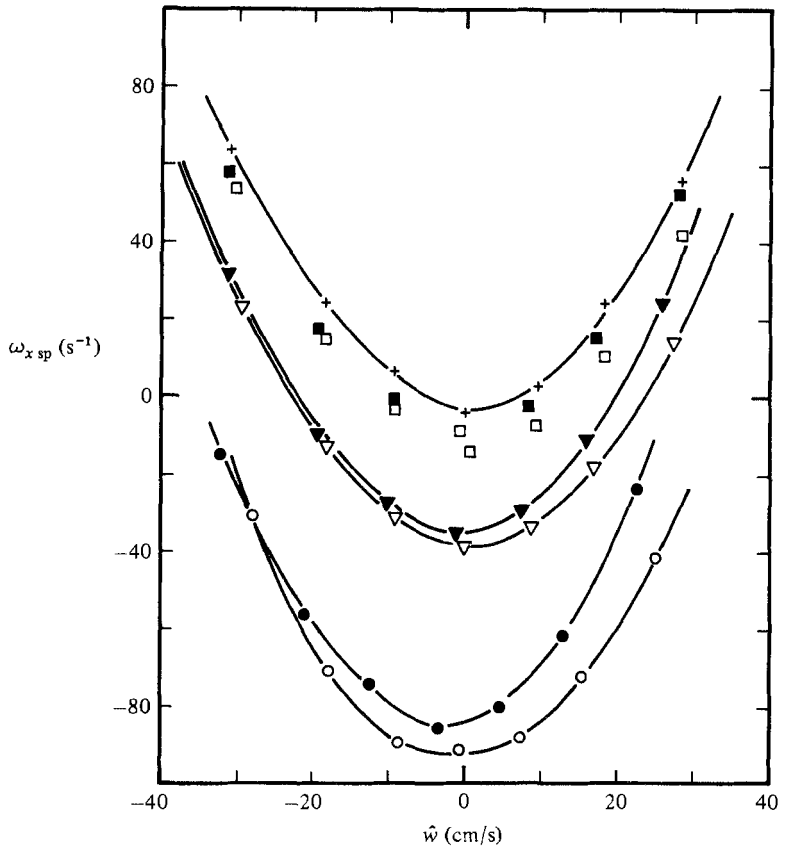

FIGURE 11. Spurious vorticity signal due to the influence of the two transverse velocity components $\hat{v}$ and $\hat{w}$ for $\bar{U} = 200$ cm/s: ■, $\hat{v} = 7.8$ cm/s; ▲, 17.1 cm/s; ●, 28.5 cm/s; +, 0 cm/s; □, −9.1 cm/s; △, −17.8 cm/s; ○, −29.5 cm/s.

recorded signals included frequencies which did not exceed about 500 Hz. In addition the mean frequency for the velocity components u, v and w – for the Reynolds number of the present work – were of the same order, i.e. about 500 Hz. Hence by digitizing all signals at a rate 1 kHz, the Nyquist sampling criterion for both the velocity components and the ω_x signal was satisfied. The sampling frequency of 1 kHz per data channel corresponds to a time between consecutive samples of about half the viscous timescale. For each wall distance 128 000 samples per channel were acquired, corresponding to a measuring time of slightly more than two minutes. Then in a second step the instantaneous values of all three velocity components and the streamwise component of vorticity were calculated. Owing to the dimension of the vorticity probe (1.9 mm, $d^+ \approx 11.5$) the minimum wall distance at which measurements are possible is $y^+ = 19$. Also, the assumptions made in deriving the equations are valid only up to this wall distance, and in this region the gradients neglected in (8) play only a minor role.

4.1. *Velocity measurements*

The mean-velocity profile measured with the new vorticity probe is shown in figure 13 with a logarithmic abscissa. As is common practice for such measurements, the mean velocity normalized with the friction velocity is represented by $u^+ = \bar{U}/u_\tau$. The

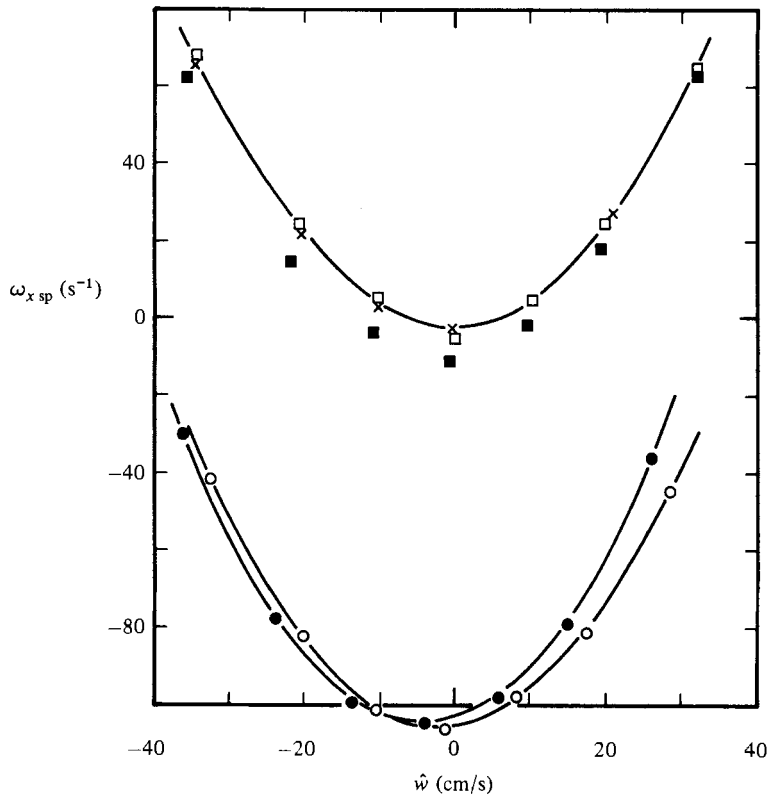

FIGURE 12. Spurious vorticity signal due to the influence of the two transverse velocity components $\hat{v}$ and $\hat{w}$ for $\overline{U} = 230$ cm/s: ■, $\hat{v} = 9$ cm/s; ●, 32.5 cm/s; ×, 0 cm/s; □, −10.5 cm/s; ○, −34.5 cm/s.

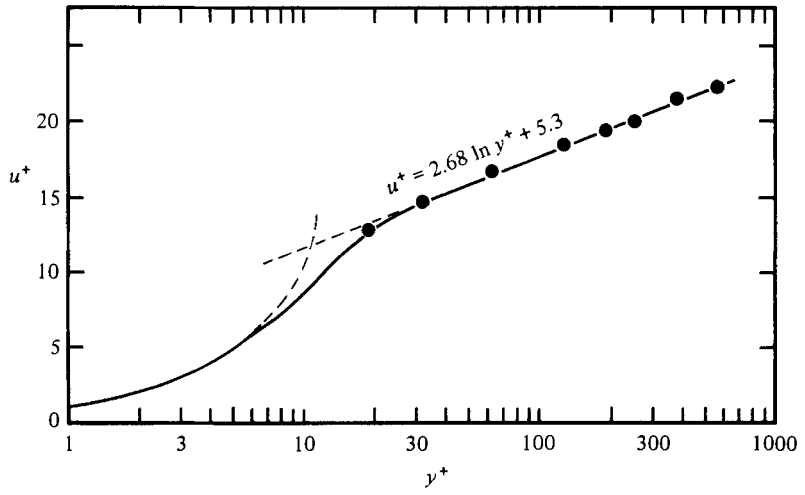

FIGURE 13. Turbulent-velocity distribution measured with the vorticity probe.

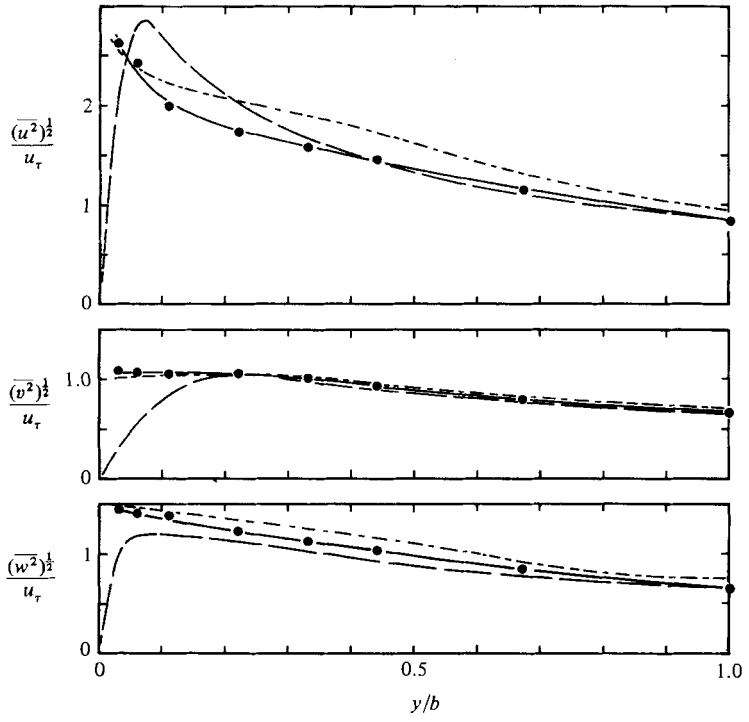

FIGURE 14. Distribution of the u-, v-, w-fluctuations normalized with the friction velocity u_τ over the channel half-width b, compared with measurements of Comte-Bellot, $Re = 57000$ (–·–) and Kreplin & Eckelmann, $Re = 7700$ (– –).

distributions of the r.m.s. values for the three fluctuating velocity components, normalized with the friction velocity u_τ, are illustrated in figure 14 along with results from Comte-Bellot (1965) and Kreplin & Eckelmann (1979*b*). The distance y from the wall is normalized here with the channel half-width b. Such a representation permits comparison of the measured values in the central region of the channel at different Reynolds numbers. In order that the measured values for different Reynolds numbers coincide near the wall, a plot as a function of y^+ is more advantageous (figure 15). Agreement between the data is good, as can also be seen in the distributions of skewness and flatness factors shown for the central region in figures 16 and 17 and for the near-wall region in figures 18 and 19.

The distributions of the normalized Reynolds stress $\overline{uv}/u_\tau^2$ and of the correlation coefficient

$$R_{uv} = \frac{\overline{uv}}{(\overline{u^2}, \overline{v^2})^{\frac{1}{2}}} \tag{9}$$

show the shape known from the literature (figure 20). The other two correlation coefficients R_{uw} and R_{vw} (their definitions are analogous to (9)) are equal to zero when the calibration method described in §3.1 is applied, and they are thus not shown here.

The results presented so far show that the new vorticity probe is well suited for velocity measurements; they also show that the velocity gradients $\partial U/\partial y$, $\partial U/\partial z$, $\partial v/\partial z$ and $\partial w/\partial y$ have only a small influence on the velocity measurements. Unfortunately, neither in Eckelmann *et al.* (1977) nor in Vukoslavcevic & Wallace (1981) are

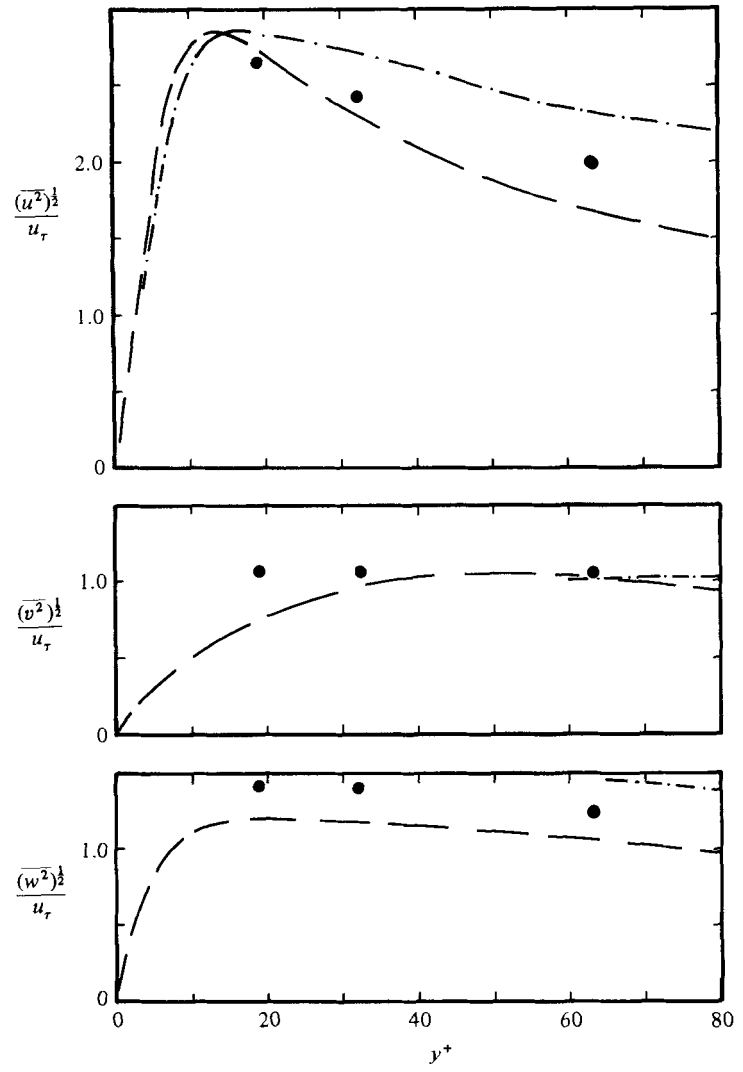

FIGURE 15. Same as figure 13 for the wall vicinity.

probabilities for the occurrence of such gradients given. As such gradients can generally result in errors for multicomponent measurements conducted with hot-wire anemometers, such errors quite probably occur in almost all measurements known from the literature. The velocity measurements described here are thus no worse and no better than previous results.

4.2. *Vorticity measurements*

The distribution of the r.m.s. values of the streamwise vorticity fluctuations over the channel half-width is shown in figure 21. The distribution near the wall is illustrated in figure 22. Dimensionless quantities were obtained by normalization with the friction velocity u_τ and the kinematic viscosity ν. This has the advantage that the limiting value (0.065) of the normalized streamwise vorticity fluctuation at the wall, as measured by Kreplin & Eckelmann (1979*b*), can also be included in this

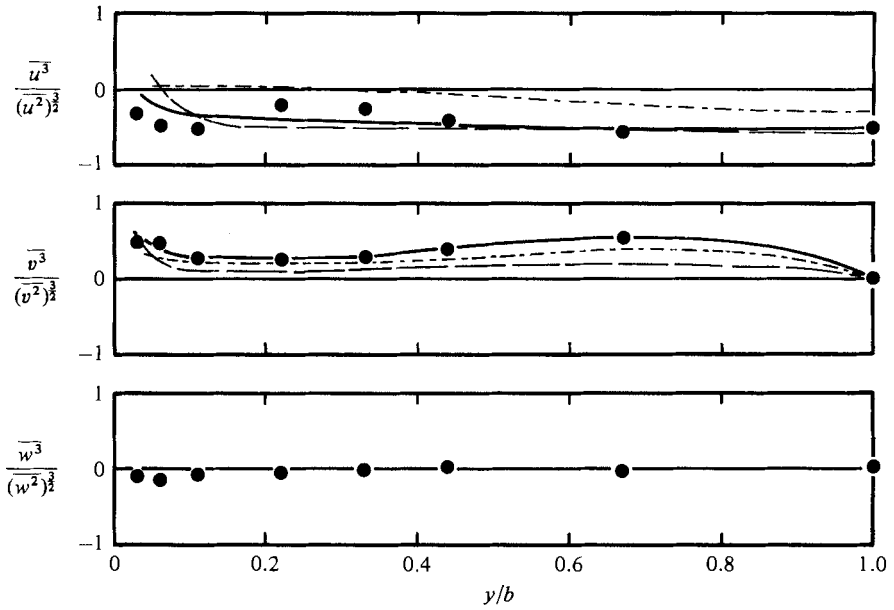

FIGURE 16. Distribution of the skewness factors for all three velocity components over the channel half-width b, compared with measurements of Comte-Bellot, $Re = 57000$ (–·–) and Kreplin & Eckelmann, $Re = 7700$ (––).

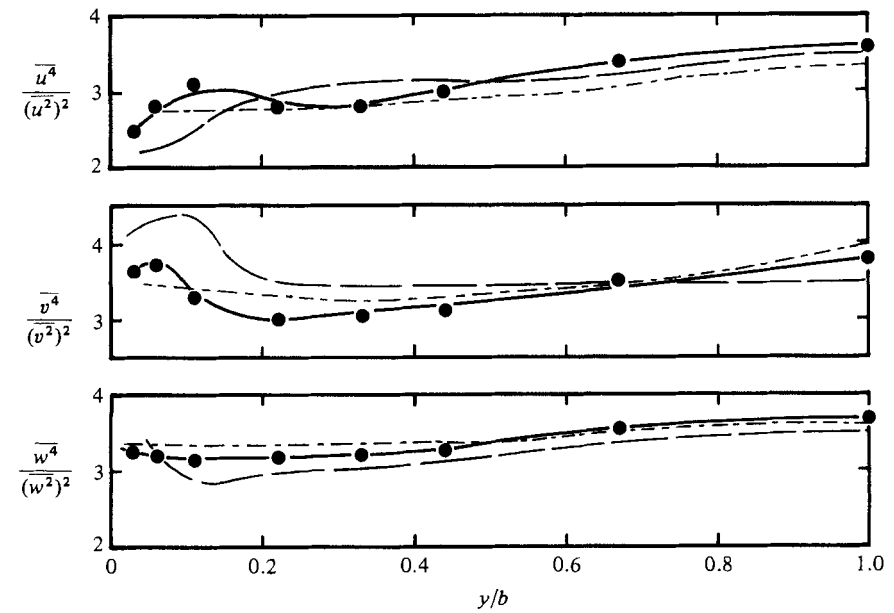

FIGURE 17. Distribution of the flatness factors for all three velocity components over the channel half-width b, compared with measurements of Comte-Bellot (–·–) and Kreplin & Eckelmann (––).

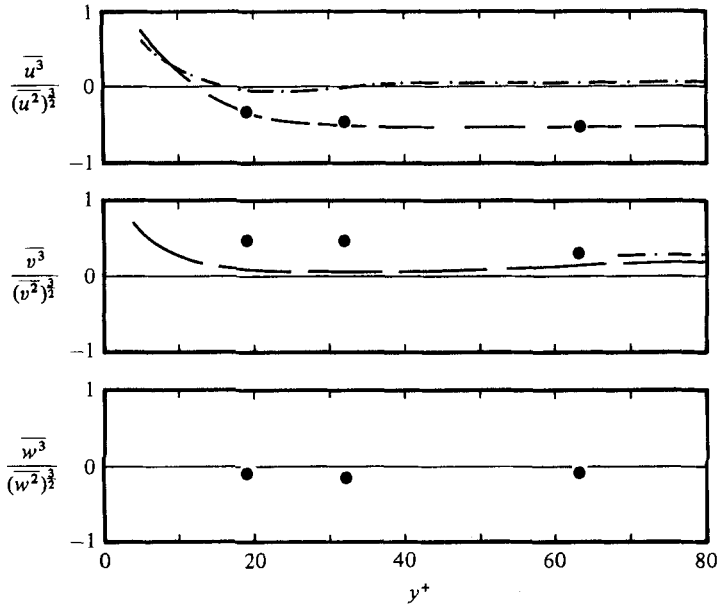

FIGURE 18. Same as figure 16 for the wall vicinity.

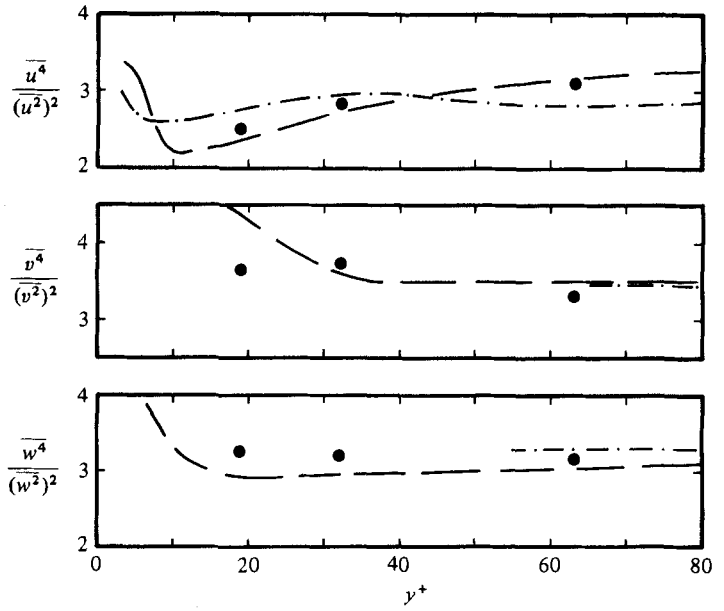

FIGURE 19. Same as figure 17 for the wall vicinity.

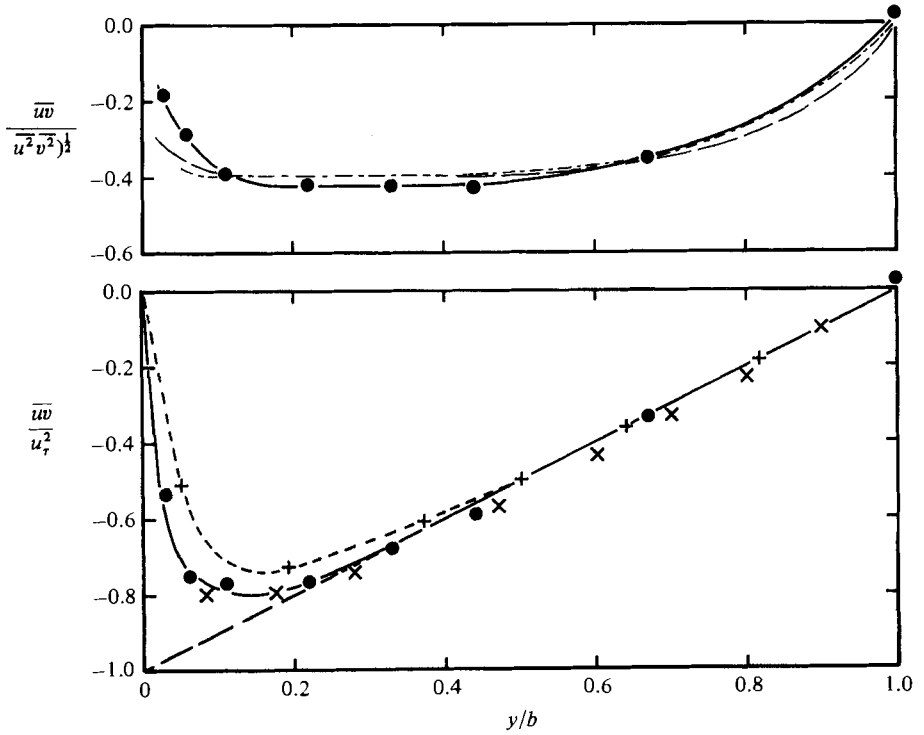

FIGURE 20. Distribution of the normalized Reynolds stress (bottom) and of the correlation coefficient over the channel half-width, b: ×, Comte-Bellot; +, Eckelmann.

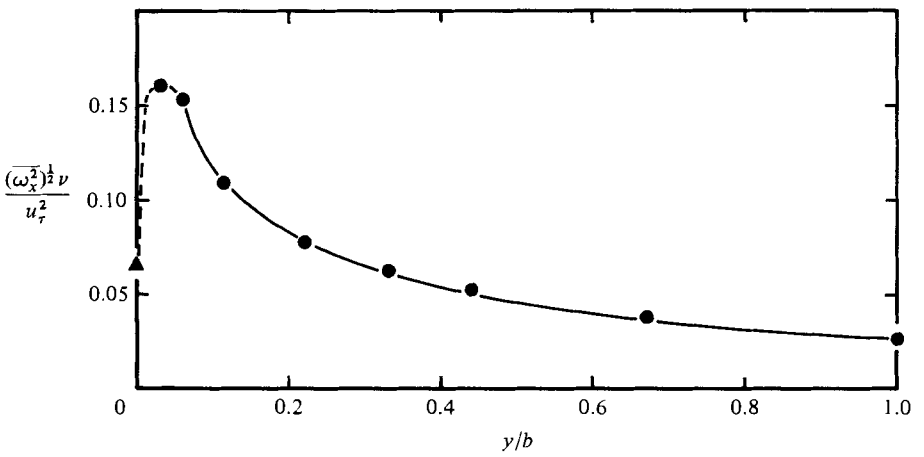

FIGURE 21. Distribution of the streamwise vorticity fluctuations normalized with the friction velocity u_τ and the kinematic viscosity of the fluid over the channel half-width b: ▲, Kreplin & Eckelmann.

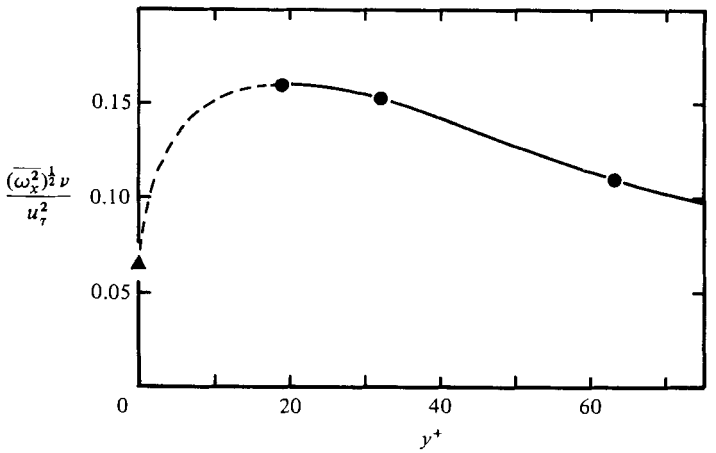

FIGURE 22. Same as figure 15 for the wall vicinity.

representation. Since the limiting values (0.115 and 0.09) at the wall measured by Py (1973) and Sirkar & Hanratty (1970) respectively are also both smaller than the value we have found at $y^+ = 19$, it must be concluded that the streamwise vorticity fluctuations attain a maximum at approximately $y^+ = 20$. This, however, does not coincide with the maximum for the streamwise velocity fluctuations $(\overline{u^2})^{\frac{1}{2}}/u_\tau$, which is found at $y^+ \approx 13$.

Figure 23 shows the distributions of skewness and flatness factors for the streamwise vorticity fluctuations. The flatness factor at the wall as measured by Kreplin & Eckelmann (1979*b*) also fits well into these results. The flatness factor for ω_x and the flatness factors for the three velocity components u, v and w exhibit similar values near the wall (figure 19); for ω_x this value increases with increasing wall distance and reaches a maximum at the centreline of about twice the value at the wall. This indicates a strongly intermittent character of vorticity at large wall distances. One can easily imagine that streamwise vortices, which are observed in the region near the wall, seldom extend out to the channel centreline.

The correlations

$$R_{u_i\omega_x} = \frac{\overline{u_i\omega_x}}{(\overline{u_i^2}\ \overline{\omega_x^2})^{\frac{1}{2}}},$$

with $i = 1, 2, 3$ where $u_1 = u$, $u_2 = v$, $u_3 = w$, were also measured with the new vorticity probe. All three correlations were found to be zero within the limits of measurement accuracy. No correlation is expected between u, v, w and ω_x in a wall-bounded turbulent flow owing to reasons of symmetry. A correlation between w and ω_x can only be expected very close to the wall, as measurements made by Kreplin & Eckelmann (1979*c*) in the viscous sublayer show that time functions of the spanwise velocity fluctuations w and the gradient $(\partial w/\partial y)|_{\mathrm{W}}$ at the wall are very similar except for a slight time shift. Owing to the relation

$$\lim_{y\to 0} \omega_x = \left.\frac{\partial w}{\partial y}\right|_{\mathrm{W}}$$

and the similarity found by Kreplin & Ecklemann, the correlation $R_{w\omega_x}$ should approach the value unity at the wall. However, no correlation between ω_x and w could

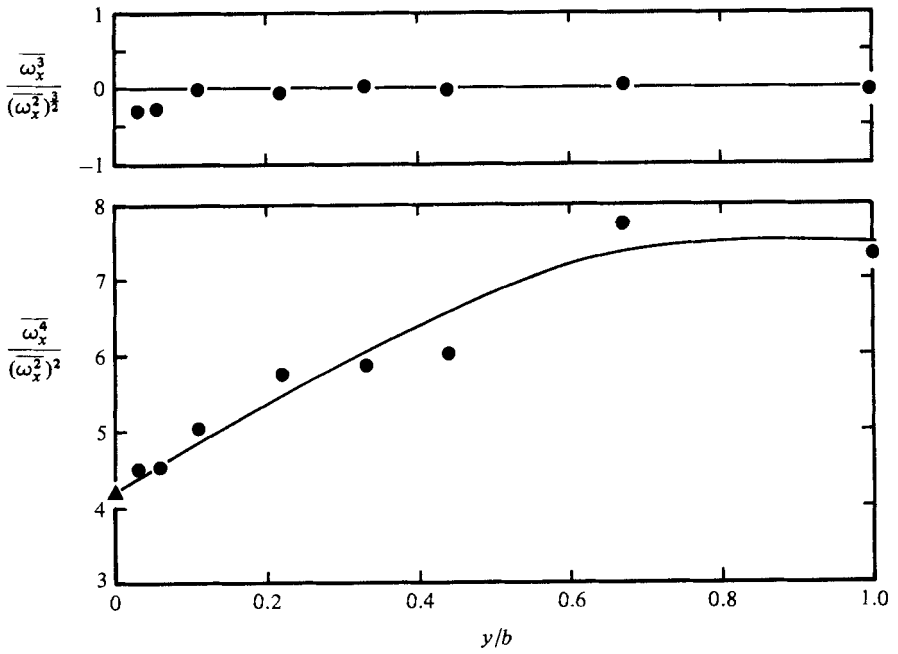

FIGURE 23. Distribution of the skewness and flatness factors for the streamwise vorticity fluctuations: ▲, Kreplin & Eckelmann.

be detected up to a wall distance of $y^+ = 19$. The fact that all three measured correlations $R_{u_i\omega_x}$ $(i = 1, 2, 3)$ are equal to zero leads to the conclusion that no crosstalk between velocity and vorticity signals exists.

5. Discussion and conclusion

Measurements of streamwise vorticity fluctuations ω_x in a turbulent channel flow have to our knowledge only been attempted by Kastrinakis with a Kovasznay-type vorticity probe in the course of his Ph.D. thesis. For details see Kastrinakis, Wallace & Willmarth (1975), Willmarth & Bogar (1977) and Kastrinakis (1977). A subsequent investigation of the Kovasznay-type probe by Kastrinakis *et al.* (1979) has shown that the ω_x signal was contaminated by all three velocity components. This result led to the design and construction of a new vorticity probe with four independently operated sensors and to the development of a new calibration technique, both of which were used for the present measurements.

The distributions of skewness and flatness factors and of r.m.s. values for the velocity fluctuations over the channel half-width measured with the new probe for all three components are in good agreement with distributions published in the literature. Also, the three correlation coefficients relating the streamwise component of vorticity to the fluctuating components of velocity are measured to be zero, as expected. This gives us confidence in our results for both the r.m.s. values and the skewness- and flatness-factor measurements of ω_x. Sirkar & Hanratty (1970), Py (1973) and Kreplin & Eckelmann (1979*b*) measured vorticity fluctuations at the wall, and Kreplin & Eckelmann measured in addition skewness and flatness factors at this position: these values all fit well as limiting values at the wall in the distribution

measured here. The distribution of the r.m.s. value for ω_x (figure 21) described in the present paper and that found earlier by Kastrinakis (1977) are quantitatively quite different. The r.m.s. values for ω_x as determined with the new probe are only about half as large as those found earlier. The location of the maximum for $(\overline{\omega_x^2})^{\frac{1}{2}}\nu/u_\tau^2$ remains unchanged at $y^+ \approx 20$, but its value changes from 0.3 to 0.16. Based on visual studies in a turbulent boundary layer Smith (1980 personal communication) has made an estimate for $|\omega_x|\nu/u_\tau^2$. He observed the most-intense streamwise vortices at $y^+ \approx 20$ and found for single vortices values in the range 0.2–0.5 at this position. The r.m.s. value of 0.16 found in the present work for the streamwise vorticity fluctuation could well be the result of such single vortices of this order of magnitude. Since the used vorticity probe averages over approximately 11.5 wall-layer units, the maximum value could be slightly higher when measured with a smaller probe.

The maximum for $(\overline{\omega_x^2})^{\frac{1}{2}}\nu/u_\tau^2$ at $y^+ \approx 20$ indicates that the occurrence of streamwise vortical structures is most probable at this position. Bakewell & Lumley (1967) derived a counter-rotating vortex pair with centre at $y^+ \approx 30$ from their velocity correlation measurements. Falco's (1980) 'pockets', which he also has interpreted as counter-rotating vortex pairs, most probably occur in the region $9 < y^+ < 23$. Also, the vortex model postulated by Blackwelder & Eckelmann (1979) has its centre at $y^+ \approx 18$ according to a later evaluation by Blackwelder (1979).

The strong increase of the flatness factor with wall distance (figure 17) indicates a strongly intermittent character for the streamwise component of vorticity in this region. The flatness factor shows values similar to those for the three fluctuating velocity components only in the vicinity of the wall, where most streamwise vortices are observed. The higher values farther away from the wall could indicate that streamwise vortices here occur sporadically. More extensive measurements are thus needed to provide further information; the new vorticity probe can be a useful tool in such an investigation.

The authors wish to thank Prof. Dr E.-A. Müller for his interest in this work. The financial support of the Max-Planck-Gesellschaft for one of the authors (E. G. K.), was greatly appreciated. We also express our gratitude to Messrs H. Hamann, K.-H. Nörtemann and H. J. Schäfer for their technical assistance, to Prof. S. G. Nychas for various fruitful discussions, to Mr F. D. Johnson for the translation and to Mrs C. Köneke for typing the manuscript.

REFERENCES

Bakewell, H. P. & Lumley, J. L. 1967 *Phys. Fluids* **10**, 1880.

Blackwelder, R. F. 1979 *AGARD Conf. Proc.* no. 271, p. 24-1.

Blackwelder, R. F. & Eckelmann, H. 1979 *J. Fluid Mech.* **94**, 577.

Brodkey, R. S. 1978 In *Proc. AFOSR Workshop on Coherent Structures in Turbulent Boundary Layers* (ed. C. R. Smith & D. E. Abbott), p. 28.

Cleveland, W. G. 1979 M.S. thesis, The University of Maryland.

Comte-Bellot, G. 1965 *Pub. Sci. Tech. du Ministère de l'Air, Paris* no. 419.

Corino, E. R. & Brodkey, R. S. 1969 *J. Fluid Mech.* **37**, 1.

Corrsin, S. 1957 *Symp. Naval Hydrodyn. Publ.* 515 NAS-NRC 373.

Corrsin, S. & Kistler, A. L. 1955 *NACA Rep.* 1244.

Eckelmann, H., Nychas, S. G., Brodkey, R. S. & Wallace, J. M. 1977 *Phys. Fluids Suppl.* **20**, S225.

Falco, R. E. 1980 In *Proc. 6th Symp. on Turbulence in Liquids, Rolla, Mo*, p. 1-1.

FRISH, M. B. & WEBB, W. W. 1981 *J. Fluid Mech.* **107**, 173.

HEAD, M. R. & BANDYOPADHYAY, P. 1981 *J. Fluid Mech.* **107**, 297.

JEROME, F. E., GUITTON, D. E. & PATEL, R. P. 1971 *Aero. Q.* **22**, 119.

KASTRINAKIS, E. G. 1977 *Max-Planck-Inst. f. Strömungsforschung Rep.* 5/1977.

KASTRINAKIS, E. G., WALLACE, J. M. & WILLMARTH, W. W. 1975 *Bull. Am. Phys. Soc.* **20**, 1442.

KASTRINAKIS, E. G., WALLACE, J. M., WILLMARTH, W. W., GHORASHI & BRODKEY, R. S. 1978 In *Structure and Mechanisms of Turbulence I* (ed. H. Fiedler). Lecture Notes in Physics, vol. 75, p. 175. Springer.

KASTRINAKIS, E. G., ECKELMANN, H. & WILLMARTH, W. W. 1979 *Rev. Sci. Instrum.* **50**, 759.

KIM, H. T., KLINE, S. J. & REYNOLDS, W. C. 1971 *J. Fluid Mech.* **50**, 133.

KISTLER, A. L. 1952 M.S. thesis, The Johns Hopkins University.

KLINE, S. J., REYNOLDS, W. C., SCHRAUB, F. A. & RUNSTADLER, P. W. 1967 *J. Fluid Mech.* **30**, 741.

KOVASZNAY, L. S. G. 1950 *Q. Prog. Rep. Aero Dept Contact* NORD-8036-JHB-3D, *The Johns Hopkins University.*

KOVASZNAY, L. S. G. 1954 *Physical Measurements in Gas Dynamics and Combustion*, p. 227. Princeton University Press.

KREPLIN, H.-P. & ECKELMANN, H. 1979*a* *Phys. Fluids* **22**, 1210.

KREPLIN, H.-P. & ECKELMANN, H. 1979*b* *Phys. Fluids* **22**, 1233.

KREPLIN, H.-P. & ECKELMANN, H. 1979*c* *J. Fluid Mech.* **95**, 305.

PRATURI, A. K. & BRODKEY, R. S. 1978 *J. Fluid Mech.* **89**, 251.

PY, B. 1973 *Intl J. Heat Mass Transfer* **16**, 129.

SIRKAR, K. K. & HANRATTY, T. J. 1970 *J. Fluid Mech.* **44**, 605.

SMITH, C. R., SCHWARTZ, S. D., METZLER, S. D. & CERRA, A. W. 1980 In *Proc. Intl Symp. on Flow Visualization, Bochum, Germany.*

THEODORSEN, T. 1952 Mechanism of turbulence. In *Proc. Midwestern Conf. Fluid Mech., 2nd Ohio State Univ., Columbus, Ohio.*

UBEROI, M. S. & CORRSIN, S. 1951 *Prog. Rep. Contract* NAW 5504 *for NACA, The Johns Hopkins University.*

VUKOSLAVCEVIC, P. & WALLACE, J. M. 1981 *Rev. Sci. Instrum.* **52**, 869.

WILLMARTH, W. W. 1975 *Adv. Appl. Mech.* **15**, 159.

WILLMARTH, W. W. & BOGAR, T. J. 1977 *Phys. Fluids Suppl.* **20**, S9.

WILLMARTH, W. W. & TU, B. J. 1967 *Phys. Fluids Suppl.* **10**, S234.

WYNGAARD, J. C. 1969 *J. Phys.* E: *Sci. Instrum.* **2**, 983.